VIP Covalent Organic Frameworks Very Important Paper
International Edition: DOI: 10.1002/anie.201912344
German Edition: DOI: 10.1002/ange.201912344

# Hot π-Electron Tunneling of Metal–Insulator–COF Nanostructures for Efficient Hydrogen Production

*Jintao Ming[+], Ai Liu[+], Jiwu Zhao, Pu Zhang, Haowei Huang, Huan Lin, Ziting Xu, Xuming Zhang, Xuxu Wang, Johan Hofkens, Maarten B. J. Roeffaers,* and Jinlin Long**

***Abstract:*** *A metal–insulator–semiconductor (MIS) photosystem based on covalent organic framework (COF) semiconductors was designed for robust and efficient hydrogen evolution under visible-light irradiation. A maximal $H_2$ evolution rate of 8.42 mmol $h^{-1}$ $g^{-1}$ and a turnover frequency of 789.5 $h^{-1}$ were achieved by using a MIS photosystem prepared by electrostatic self-assembly of polyvinylpyrrolidone (PVP) insulator-capped Pt nanoparticles (NPs) with the hydrophilic imine-linked TP-COFs having =C=O···H–N= hydrogen-bonding groups. The hot π-electrons in the photoexcited n-type TP-COF semiconductors can be efficiently extracted and tunneled to Pt NPs across an ultrathin PVP insulating layer to reduce protons to $H_2$. Compared to the Schottky-type counterparts, the COF-based MIS photosystems give a 32-fold-enhanced carrier efficiency, attributed to the combined enhancement of photoexcitation rate, charge separation, and oxidation rate of holes accumulated in the valence band of the TP-COF semiconductor.*

Hydrogen production by photocatalytic or photoelectrochemical water splitting is an attractive means to convert intermittent solar radiation into a storable, clean fuel. Tremendous effort has been devoted to developing efficient and stable inorganic semiconductor materials for this purpose, including silicon, various oxides, graphitic carbon nitrides, metal–organic frameworks, and III–V compounds.[1] Recently, covalent organic frameworks (COFs) as a new class of crystalline organic materials, have started to further expand the availability of photoactive materials. The ordered architecture permitted the electronic structure and chemical functionality of COFs to be tailored and regulated at molecular level. Therefore, construction of crystalline COFs with suitable photoactive building blocks and layered stacking sequences is an exciting direction with great potential to achieve highly active new-generation artificial photosystems.

To date, few kinds of COFs was active for solar-to-chemical energy conversion and photoredox catalysis, besides the triazine-based COFs that were shown first by Lotsch and co-workers in 2014 to be active for photocatalytic hydrogen production in the presence of Pt as a proton reduction catalyst.[2] Much attention has been paid to simply adjust the component and electronic structure of triazine-based COFs for the target applications in photocatalytic hydrogen production, $CO_2$ reduction, and organic transformations.[3,4] One exceptional example is the sulfone-containing COFs reported recently by Cooper and co-workers.[4] A maximum $H_2$ evolution rate of 10.1 mmol $g^{-1}$ $h^{-1}$ was obtained with $\lambda \geq$ 420 nm (hereafter called visible light) excitation using ascorbic acid (AA) as sacrificial agent and photodeposited Pt (from $H_2PtCl_6$) as the hydrogen-evolving catalyst. The formed Schottky junction at the contact interface of Pt/COFs can improve the separation and transfer of photogenerated charges confined in organic π-orbits, which is the key step to enable the hydrogen production, but the overall efficiency is utterly inadequate for the practical application. Fast extraction of charge carriers from the photoexcited COFs is of most importance for the efficient photoredox catalysis, and yet highly formidable.

In this work, we proposed first a charge tunneling strategy to extract hot π-electrons from photoexcited COF semiconductors and designed smartly a metal–insulator–semiconductor (MIS) nanostructured photosystem to demonstrate clearly the high-efficiency solar-to-hydrogen fuel production. As illustrated in Figure 1 A, a typical MIS junction consists of a metallic electron collector situated on the surface of an insulating oxide-covered semiconductor.[5] When the MIS heterostructure is illuminated, electrons can tunnel through the insulating thin layer (commonly ca. 1.0 nm) to the collector, where the hydrogen evolution reaction (HER) takes place. It requires a high-quality interface to eliminate the interfacial band-offset energies of elemental and compound semiconductors.[5a,d] Given the structural characteristics of COFs semiconductors, the uniform distribution of metallic collectors in the ordered pores is necessary for collecting π-electrons emitted from the skeleton of COFs. Moreover, the insulators with a strong chemical affinity for both metallic and organic components (C, N, and O) are

[*] J. Ming,[+] A. Liu,[+] Dr. J. Zhao, Dr. P. Zhang, Dr. H. Lin, Z. Xu, Prof. X. Wang, Prof. J. Long
State Key Laboratory of Photocatalysis on Energy and Environment
Fuzhou University, Fuzhou, 350116 (P. R. China)
E-mail: jllong@fzu.edu.cn
Dr. H. Huang, Prof. M. B. J. Roeffaers
Centre for Membrane Separation, Adsorption, Catalysis and Spectroscope for Sustainable Solutions (cMACS), KU Leuven
Celestijnenlaan 200F, 3001 Heverlee (Belgium)
E-mail: maarten.roeffaers@kuleuven.be
Prof. X. Zhang
Department of Applied Physics
The Hong Kong Polytechnic University
Hong Kong 999077 (China)
Prof. J. Hofkens
Department of Chemistry, Faculty of Sciences, KU Leuven
Celestijnenlaan 200F, 3001 Heverlee (Belgium)
[+] These authors contributed equally to this work.
Supporting information and the ORCID identification number(s) for the author(s) of this article can be found under: https://doi.org/10.1002/anie.201912344.

  

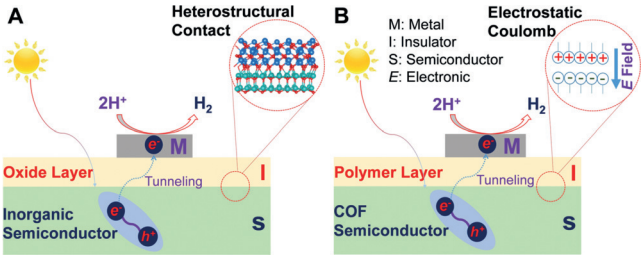


***Figure 1.*** Photoexcited electron tunneling in metal–insulator–semiconductor nanostructures for water reduction. A) Classical model of inorganic MIS heterostructures with an ultrathin oxide tunneling layer and inorganic semiconductor; B) the organic MIS nanostructured photocatalysts with a COF semiconductor assembled with polymer-capped Pt NPs.

preferential for maximizing the π-electron tunneling efficiency. Water-soluble polymers, especially polyvinylpyrrolidone (PVP), are the perfect candidate insulators, which were often used for the controlled synthesis of metal nanoparticles (NPs), including Au, Pt, Ag, and Pd with a low HER overpotential.[6] The surface of metal NPs is covered with an ultrathin capping layer of polymeric insulator, and thus they can be homogeneously dispersed in aqueous solution. One important point is that the polymer-capped metal NPs, especially Pt, are usually charged.[6b] An electrostatic self-assembly method was therefore employed to construct the COF-based MIS photosystems with the insulating polymer. As shown in Figure 1 B, an electrostatic field normal to COFs is expectedly formed between COFs and insulators, decreasing drastically the binding energy of organic excitons.

For addressing fully this pressing issue, we designed and synthesized two D-A type COFs to construct MIS photosystems by the self-assembly strategy. As depicted in Figure 2 A, one is denoted as TP-COF, composed of 2,4,6-triformylphloroglucinol (TP) acceptor and 1,4-phenylenediamine (PDA) donor, and another is called as BT-COF, consisting of 1,3,5-benzenetricarboxaldehyde (BT) acceptor and the PDA donor. The powder X-ray diffraction (XRD) patterns of the TP-COF and BT-COF materials (Figure 2 B,C) exhibited several strong diffraction peaks indexed to the hexagonal crystalline phase in the region of 1.5–10°.[7] The peak at ca. 4.73° is assigned to the {100} plane.[7a] According to the Bragg equation ($d = n\lambda/2\sin\theta$), the pore diameter ($d$) is about 1.87 nm, coincident to the theoretical value (1.83 nm). The {100} plane is fully horizontal for the two COFs, showing the long-range 2D π-conjugation. The peaks ascribed to the {110} and {200} planes are positioned, respectively, at about

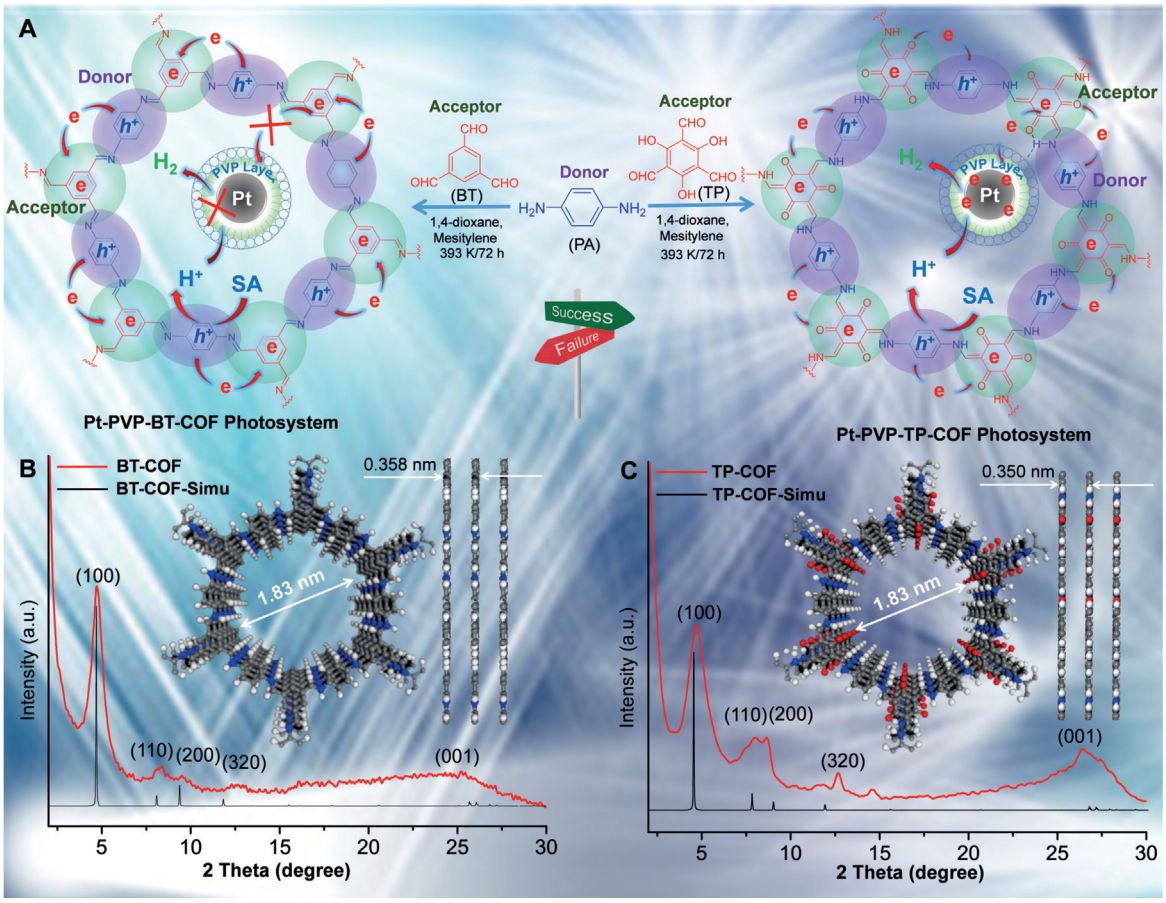


***Figure 2.*** A) Illustration of Pt-PVP-COFs photosystems for efficient photocatalytic hydrogen production in the presence of a sacrificial agent (**SA**). B) The XRD pattern of the as-prepared BT-COF and its optimized structure and A-A stacking analysis along the {001} direction by the DFT calculations. C) The XRD pattern of the as-prepared TP-COF and its optimized structure and A-A stacking analysis along the {001} direction by the DFT calculations.

  

8.0° and 8.7° for TP-COF, but at about 8.4° and 9.5° for BT-COF. All of the small angular diffraction peaks are in good agreement with the corresponding simulated results according to the A-A stacking model. The peaks at ca. 12.7° for TP-COF and about 12.5° for BT-COF are indexed to the {320} plane originated from the A-B stacking model. The peaks centered at 25–27° originate from the {001} plane of the layered COFs. The interlamellar spacing is calculated to be about 0.338 nm for TP-COF (ca. 26.4°) and about 0.352 nm for BT-COF (ca. 25.3°). These results indicated the successful synthesis of crystalline COFs through the direct amine–aldehyde condensation reaction.

Next, Fourier transform infrared (FTIR), $^{13}C$ solid-state nuclear magnetic resonance (NMR), and X-ray photoelectric (XPS) spectroscopies were used to study further the structure and chemical states of TP-COF and BT-COF. The FTIR spectra of TP-COF and BT-COF are shown in the Supporting Information, Figure S1. It appears that after the condensation reaction, besides the bands belonging to C–H groups and benzene rings, three characteristic vibrational bands corresponding to N–H groups of the PDA donor at 3376, 3296 and 3202 $cm^{-1}$ disappear in the FTIR spectra, and the C=O vibrational bands of TP and BT positioned, respectively, at 1690 and 1640 $cm^{-1}$ decrease greatly in intensity. Two new bands ascribed to C=C groups appear at 1573 and 1450 $cm^{-1}$ for TP-COF, suggesting the formation of the covalent C–N linkage and the transform of C–OH into C=O in the TP blocks. In contrast, a new band belonging to C=N is discernable at 1618 $cm^{-1}$ for BT-COF, indicating the formation of covalent C=N linkage in the BT blocks. Furthermore, it appears from the $^{13}C$ NMR spectra (Supporting Information, Figure S2) that the characteristic peaks belonging to the C–N and C=N linkages occur, respectively, at about 146 and about 157 ppm (marked as b), and the signal at 181–184 ppm (marked as a) is a direct indicative of the formation of C=O bonds in TP-COF.[7a] The N 1s spectra (Supporting Information, Figure S3A) showed only one core level peak at 399.4 eV for TP-COF and 398.4 eV for BT-COF, attributed unambiguously to the pyrrolic nitrogen species (=NH) and the pyridinic nitrogen species (C=N–C),[8] respectively, proving the $sp^2$ covalent C–N bonding in TP-COF and the $sp^2$ covalent C=N bonding in BT-COF. The C 1s core level peaks are at 288.7 and 286.4 eV, corresponding to the carbon atoms of C=O and C=C bonds, respectively. The O 2p binding energy of the C=O bonds is at 532.1 eV (Supporting Information, Figure S3B). These characterization results showed the structural difference between BT-COF and TP-COF.

The ultraviolet-visible diffuse reflectance (UV/Vis DRS) spectra (Supporting Information, Figure S4A) of the TP-COF and BT-COF photoabsorbers showed clearly an absorption band edge with the semiconducting feature at ca. 615 nm for TP-COF and 592 nm for BT-COF, corresponding to the band-gap energies of 1.97 and 2.12 eV, respectively (Supporting Information, Figure S4B). The density functional theory (DFT) calculations indicated the n-type semiconducting feature because the Fermi levels of the two COF semiconductors are very close to the conduction band (CB) bottoms (Supporting Information, Figure S5). The Mott–Schottky plots gave the positive slope of the linear plots (Supporting Information, Figure S6A), confirming the above-mentioned conclusion. The TP-COF has a flat band potential of −0.25 eV vs. RHE, which is more positive than that (−0.61 eV vs. RHE) of the BT-COF. Their valence band (VB) potentials are more positive than the potential of the one-hole oxidation of ascorbic acid and the oxygen evolution potential of $O_2/H_2O$ (+1.23 eV vs. RHE; Supporting Information, Figure S6B), indicating the feasibility of photocatalytic water splitting over the COF semiconductors.

Unexpectedly, owing to the different framework components, upon dispersion in aqueous solution, the TP-COF suspension represented a negatively charged colloid property (−24.61 mV), which is remarkably different from the BT-COF counterpart (+7.12 mV; Supporting Information, Figure S7). The adjacent C=O and =N–H groups in nanopores of TP-COF formed easily intramolecular hydrogen bonds (Figure 2A), offering a large amount of adsorption sites to assemble with the positively-charged PVP-Pt NPs that have a zeta potential of +31.45 mV (Supporting Information, Figure S7) and a coverage size of about 1.3 nm (Supporting Information, Figure S8). The majority of them are difficult to access into the nanopores of COFs, positioning accordingly at the orifices upon the electrostatic self-assembly. Figure 3A and B shows the transmission electron microscopy (TEM) patterns of the resulting assemblies, Pt-PVP-TP-COF and Pt-PVP-BT-COF. It appears that a majority of PVP-Pt NPs were highly dispersed on the TP-COF surface, while few Pt NPs are discernible on the surface of BT-COF substrate. A majority of Pt NPs are distributed around the BT-COF particles owing to the charge-repulsion. The result indicated that the preparation of MIS nanostructured photosystem, COF-polymer-Pt, is successful with TP-COF, and yet fails for BT-COF. Therefore, they displayed an expected huge difference in photocatalytic hydrogen production.

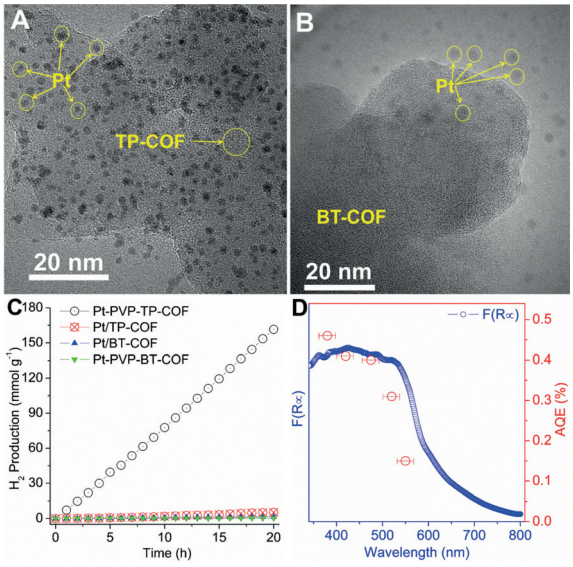


***Figure 3.*** A),B) TEM patterns of as-prepared Pt-PVP-TP-COF (A) and Pt-PVP-BT-COF (B) samples. C) Photocatalytic hydrogen evolution under visible light irradiation in the presence of ascorbic acid. D) Action spectrum of the TP-COF for hydrogen production.

Figure 3C shows the photocatalytic hydrogen evolution under visible light irradiation by using AA as a sacrificial electron donor. The Pt-PVP-BT-COF photosystem only produces a detectable amount of hydrogen within 20 h, is worse than the Pt/BT-COF photocatalyst with a low hydrogen evolution rate of ca. 76.0 umol $g^{-1}$ $h^{-1}$. Impressively, the Pt-PVP-TP-COF photosystem demonstrates a linear and stable increase in hydrogen evolution with illumination time at a hydrogen production rate of 8.42 mmol $h^{-1}$ $g^{-1}$, which is 32-fold higher than the corresponding the Mott–Schottky photocatalyst, Pt/TP-COF, with a low hydrogen production rate of about 265 umoL $g^{-1}$ $h^{-1}$. The turnover frequency (TOF) of 789.5 $h^{-1}$ was recorded with the Pt-PVP-TP-COF photosystem (Supporting Information, Table S1). The results indicated clearly that the MIS photosystem more efficiently transports the photoexcited π-electrons from the TP-COF semiconductor to Pt NPs, as comparison with the Schottky junction that features the interfacial contact between COFs and Pt NPs, as demonstrated by TEM images (Supporting Information, Figure S9). The apparent quantum efficiency (AQE) of about 0.4% at about 475 nm was achieved, as depicted in Figure 3D. The AQE values of the Pt-PVP-TP-COF photosystem matched basically with the UV/Vvis DRS of the TP-COF photoabsorber. It implied the promising perspective of electron tunneling in MIS nanostructures for enhancement of the hydrogen production.

To probe the physical mechanism of the TP-COF-based MIS photosystem for efficient hydrogen production, we performed photoluminescence (PL) measurements (Figure 4A). TP-COF showed a broad PL peak centered at about 640 nm. It can be divided into two peaks positioned, respectively, at 622 and 710 nm. The PL peak at 622 nm was resulted from the band-gap radiative recombination and the 710 nm emission was contributed from the π–π interactions between layers of COFs.[9] The significantly enhanced emission at 622 nm was observed for Pt-PVP-TP-COF owing to the interaction of metals with the adjacent fluorophores, which improves drastically the photoexcitation rate.[10] The two emissions were quenched for Pt/TP-COF because a majority of photogenerated carriers in TP-COF were transferred across the interfacial Mott–Schottky junction to Pt NPs, where the non-radiative recombination takes place. As a result, the photocurrent response (Figure 4B) corresponded perfectly to the PL results, giving an order of Pt-PVP-TP-COF > TP-COF > Pt/TP-COF. The lifetime results (Supporting Information, Figure S10) further confirmed the conclusions. Therefore, the charge dynamics and hydrogen evolution mechanism can be depicted clearly in Figure 4C for the Mott–Schottky photocatalyst and Figure 4D for the MIS photocatalyst. The proposed models can explain well the tremendous difference in hydrogen evolution rate. It appears that for the Schottky-type photocatalyst, the non-radiative recombination occurring on Pt NPs is detrimental greatly to the HER reaction because of the significant decrease in effective hot carriers and hole oxidation. In contrast, the photogenerated holes in the MIS photosystem cannot be transferred to Pt NPs but be accumulated predominantly in TP-COF to accelerate kinetically the one-hole oxidation of AA to produce protons. The energetic π-electrons can be smoothly tunneled to Pt NPs with the aid of electrostatic field, consequently achieving the more efficient charge separation and larger photoexcitation rate. Another two MIS counterparts shown in the Supporting Information, Figure S11 were prepared by the same strategy to further confirm the superiority of COF-based MIS nanostructures to photocatalytic hydrogen production.

In summary, this study demonstrated the efficient hot π-electron tunneling of organic MIS nanostructures for solar hydrogen fuel production. The MIS photosystems are well established to be superior to the Schottky-type counterparts. The efficiency of the former is 32-fold higher than the latter. The maximal $H_2$ evolution rate reached 8.42 mmol $h^{-1}$ $g^{-1}$ and the highest apparent quantum efficiency is up to 0.4% at 475 nm using TP-COF as visible light antenna. The characterization results indicated that the MIS nanostructures can not only enhance the photoexcitation of the semiconductor moiety and the charge separation but promote the hole-oxidation and accelerate the HER reaction. This work not only clearly reveals the promising potential of MIS nanostructures for hydrogen fuel production but provides a conceptual guide to the design of novel COF semiconductors to construct artificial photosystems.

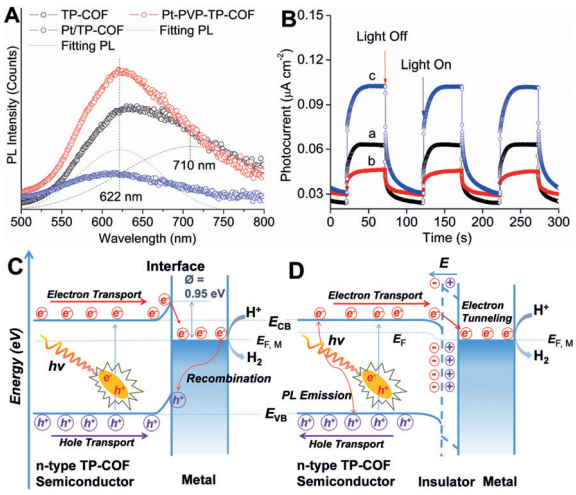


***Figure 4.*** A) Fluorescence spectra under 357 nm excitation. B) Short-circuit photocurrent response of a) TP-COF, b) Pt/TP-COF, and c) Pt-PVP-TP-COF photocatalysts under visible-light irradiation. C),D) The charge dynamics and hydrogen production mechanism on the C) Mott–Schottky Pt/TP-COF and D) Pt-PVP-TP-COF MIS photocatalysts.

## Acknowledgements

This work was financially supported by the NSFC (Grants No. 21773031), the Natural Science Foundation of Fujian Province of P. R. China (2018J01686), the Science and Technology Project of Education Office of Fujian Province of P.R. China (JT180020), and the State Key Laboratory of Photocatalysis on Energy and Environment (SKLPEE-2017A01 and SKLPEE-2017B02).

  

## Conflict of interest

The authors declare no conflict of interest.

**Keywords:** covalent organic frameworks · hydrogen production · photocatalysis · nanostructures · semiconductors

**How to cite:** *Angew. Chem. Int. Ed.* **2019**, *58*, 18290–18294
*Angew. Chem.* **2019**, *131*, 18458–18462

[1] a) T. Hisatomi, J. Kubota, K. Domen, *Chem. Soc. Rev.* **2014**, *43*, 7520–7535; b) T. Zhou, Y. Du, A. Borgna, J. Hong, Y. Wang, J. Han, W. Zhang, R. Xu, *Energy Environ. Sci.* **2013**, *6*, 3229–3234; c) Y. Hou, B. L. Abrams, P. C. K. Vesborg, M. E. Björketun, K. Herbst, L. Bech, A. M. Setti, C. D. Damsgaard, T. Pedersen, O. Hansen, J. Rossmeisl, S. Dahl, J. K. Nørskov, I. Chorkendorff, *Nat. Mater.* **2011**, *10*, 434–438; d) X. Wang, K. Maeda, A. Thomas, K. Takanabe, G. Xin, J. M. Carlsson, K. Domen, M. Antonietti, *Nat. Mater.* **2009**, *8*, 76–80.

[2] L. Stegbauer, K. Schwinghammer, B. V. Lotsch, *Chem. Sci.* **2014**, *5*, 2789–2793.

[3] a) M. Bhadra, S. Kandambeth, M. K. Sahoo, M. Addicoat, E. Balaraman, R. Banerjee, *J. Am. Chem. Soc.* **2019**, *141*, 6152–6156; b) S. Yang, W. Hu, X. Zhang, P. He, B. Pattengale, C. Liu, M. Cendejas, I. Hermans, X. Zhang, J. Zhang, J. Huang, *J. Am. Chem. Soc.* **2018**, *140*, 14614–14618; c) P.-F. Wei, M.-Z. Qi, Z.-P. Wang, S.-Y. Ding, W. Yu, Q. Liu, L.-K. Wang, H.-Z. Wang, W.-K. An, W. Wang, *J. Am. Chem. Soc.* **2018**, *140*, 4623–4631; d) W. Zhong, R. Sa, L. Li, Y. He, L. Li, J. Bi, Z. Zhuang, Y. Yu, Z. Zou, *J. Am. Chem. Soc.* **2019**, *141*, 7615–7621.

[4] X. Wang, W.-H. Zhu, L. Chen, S. Y. Chong, M. A. Little, Y. Wu, R. Clowes, Y. Yan, M. A. Zwijnenburg, R. S. Sprick, A. I. Cooper, *Nat. Chem.* **2018**, *10*, 1180–1189.

[5] a) T. Zhu, M. N. Chong, *Nano Energy* **2015**, *12*, 347–373; b) D. V. Esposito, I. Levin, T. P. Moffat, A. A. Talin, *Nat. Mater.* **2013**, *12*, 562–568; c) L. Ji, H.-Y. Hsu, X. Li, K. Huang, Y. Zhang, J. C. Lee, A. J. Bard, E. T. Yu, *Nat. Mater.* **2017**, *16*, 127–131; d) I. A. Digdaya, G. W. P. Adhyaksa, B. J. Trzesniewski, E. C. Garnett, W. A. Smith, *Nat. Commun.* **2017**, *8*, 15968; e) J. C. Hill, A. T. Landers, J. A. Switzer, *Nat. Mater.* **2015**, *14*, 1150–1155.

[6] a) K. M. Koczkur, S. Mourdikoudis, L. Polavarapu, S. E. Skrabalak, *Dalton Trans.* **2015**, *44*, 17883–17905; b) H. Lin, D. Liu, J. Long, Z. Zhang, H. Zhuang, Y. Zheng, X. Wang, *Phys. Chem. Chem. Phys.* **2015**, *17*, 10726–10736; c) L. Pastoriza-Santos, L. M. Liz-Marzán, *Langmuir* **2002**, *18*, 2888–2894.

[7] a) S. Kandambeth, A. Mallick, B. Lukose, M. V. Mane, T. Heine, R. Banerjee, *J. Am. Chem. Soc.* **2012**, *134*, 19524–19527; b) A. P. Côté, A. I. Benin, N. W. Ockwig, M. O'Keeffe, A. J. Matzger, O. M. Yaghi, *Science* **2005**, *310*, 1166–1170.

[8] a) L. Guo, Y. Niu, H. Xu, Q. Li, S. Razzaque, Q. Huang, S. Jin, B. Tian, *J. Mater. Chem. A* **2018**, *6*, 19775–19781; b) J. Long, X. Xie, J. Xu, Q. Gu, L. Chen, X. Wang, *ACS Catal.* **2012**, *2*, 622–631.

[9] a) S. Dalapati, E. Jin, M. Addicoat, T. Heine, D. Jiang, *J. Am. Chem. Soc.* **2016**, *138*, 5797–5800; b) S. Wan, J. Guo, J. Kim, H. Ihee, D. Jiang, *Angew. Chem. Int. Ed.* **2008**, *47*, 8826–8830; *Angew. Chem.* **2008**, *120*, 8958–8962; c) A. C. Jakowetz, T. F. Hinrichsen, L. Ascherl, T. Sick, M. Calik, F. Auras, D. D. Medina, R. H. Friend, A. Rao, T. Bein, *J. Am. Chem. Soc.* **2019**, *141*, 11565–11571.

[10] J. R. Lakowicz, K. Ray, M. Chowdhury, H. Szmacinski, Y. Fu, J. Zhang, K. Nowaczyk, *Analyst* **2008**, *133*, 1308–1346.

Manuscript received: September 26, 2019
Accepted manuscript online: October 23, 2019
Version of record online: November 12, 2019

  